Emergence of the physiological effects of elevated CO_2 on land-atmosphere exchange of carbon and water

Chunhui Zhan[1], René Orth[1], Mirco Migliavacca[1,4], Sönke Zaehle[2], Markus Reichstein[1], Jan Engel[2], Anja Rammig[3] and Alexander J. Winkler[1]

[1] Department for Biogeochemical Integration, Max Planck Institute for Biogeochemistry, Jena, Germany
[2] Department of Biogeochemical Signals, Max Planck Institute for Biogeochemistry, Jena, Germany
[3] Land Surface-Atmosphere Interactions, Technical University of Munich, TUM School of Life Sciences Weihenstephan, 85354 Freising, Germany
[4] European commission, Joint Research Centre, Ispra (VA), Italy

Abstract

Elevated atmospheric CO_2 (eCO_2) influences the carbon assimilation rate and stomatal conductance of plants, and thereby can affect the global cycles of carbon and water. However, the extent to which these physiological effects of eCO_2 influence the land-atmosphere exchange of carbon and water is uncertain. In this study, we aim at developing a method to detect the emergence of the physiological CO_2 effects on various variables related to carbon and water fluxes. We use a comprehensive process-based land surface model QUINCY (QUantifying Interactions between terrestrial Nutrient CYcles and the climate system) to simulate the leaf-level effects of increasing atmospheric CO_2 concentrations and their century-long propagation through the terrestrial carbon and water cycles across different climate regimes and biomes. We then develop a statistical method based on the signal-to-noise ratio to detect the emergence of the eCO_2 effects. The signal in gross primary production (GPP) emerges at relatively low eCO_2 ($\Delta[CO_2]$ ~ 20 ppm) where the leaf area index

(LAI) is relatively high. Compared to GPP, the eCO_2 effect causing reduced transpiration water flux (normalized to leaf area) emerges only at relatively high CO_2 increase ($\Delta[CO_2] >> 40$ ppm), due to the high sensitivity to climate variability and thus lower signal-to-noise ratio. In general, the response to eCO_2 is detectable earlier for variables of the carbon cycle than the water cycle, when plant productivity is not limited by climatic constraints, and stronger in forest-dominated rather than in grass-dominated ecosystems. Our results provide a step towards when and where we expect to detect physiological CO_2 effects in in-situ flux measurements, how to detect them and encourage future efforts to improve the understanding and quantification of these effects in observations of terrestrial carbon and water dynamics.

1 Introduction

Plants are tightly coupled to the ambient atmosphere through their exchange of energy, water and carbon (Gentine et al., 2019). Through this coupling, plants play an essential role in controlling the global cycles of carbon and water, and also modulate Earth's surface energy balance (Gedney et al., 2006; Williams and Torn, 2015; Friedlingstein et al., 2019). Changing atmospheric conditions such as rising air temperature, or increasing dryness in turn directly impact on plants and their functioning (Reichstein et al., 2013; Novick et al., 2016; Bastos et al., 2020). Also changes in the atmospheric composition, such as elevated atmospheric CO_2 (eCO_2) can alter plant productivity, for example by stimulating carbon assimilation and by reducing stomatal conductance (Ainsworth and Long, 2005; Norby and Zak, 2011; Walker et al., 2021). As a result, the light-use efficiency (LUE; Drake et al., 1997) and the water-use efficiency of plants (WUE; Peñuelas et al., 2011; Ueyama et al., 2020)

increase under eCO_2. The combined effect is referred to as the CO_2 fertilization effect (Körner et al., 2007; Walker et al., 2021).

Plant leaves respond directly to eCO_2 through the physiological mechanisms associated to the CO_2 fertilization effect, which could potentially translate into changes of gross primary productivity (GPP) and transpiration (Tr) that can propagate further into the carbon and water cycles (Fernández-Martínez et al., 2017; Lemordant et al., 2018; Walker et al., 2021). Specifically, the eCO_2 effect alters the carbon cycle by triggering changes in GPP resulting in changes in net primary production (NPP) and various aspects of biomass production, accumulation and allocation (e.g., leaves or roots). The increased biomass production can potentially contribute to an increased leaf area index (LAI). Observational evidence suggests that this effect can vary substantially across different biomes and plant functional types (Norby and Zak, 2011; De Kauwe et al., 2014; Winkler et al., 2021). The water cycle is affected as eCO_2 is triggering changes in the leaf-level Tr flux which controls the largest fraction of the land-atmosphere water exchange (Good et al., 2015). The eCO_2-induced change of Tr implies a potential influence on other components in the water cycle, such as soil evaporation, run-off, and consequently soil moisture (Leuzinger and Körner, 2007; Lemordant et al., 2018). However, reduced transpiration at the leaf level due to reduced stomatal conductance and stomatal density in response to eCO_2 (Woodward and Kelly, 1995; Ainsworth and Rogers, 2007) could be offset by a simultaneous increase in leaf area, and thus transpiration at canopy level as more carbon is invested in leaf growth in response to eCO_2 (Wullschleger et al., 2002). These competing effects of eCO_2 could potentially compensate each other, resulting in a non-detectable effect on the water cycle. Similar but in an opposite way, the increasing leaf area enhances GPP by controlling light interception (McCarthy et al., 2006).

The quantification of the effects of eCO_2 on carbon and water cycles in experiments and observations remain inconsistent. The intrinsic WUE inferred from 21 flux site measurements shows strong increase (Keenan et al., 2013), while the study by Knauer et al. (2017) indicates a smaller magnitude of WUE response at a recent large scale. Increased biomass is found in many Free-Air CO_2 Enrichment (FACE) experiments (Walker et al., 2019). However, tree-ring studies indicate the increased intrinsic WUE does not translate into the increased tree biomass (Peñuelas et al., 2011; van der Sleen et al., 2015). The diverse response of plant physiology to eCO_2 is observed in many other aspects. Results from field experiments show the magnitude of eCO_2 stimulation on carbon assimilation rate varies considerably across species and experimental conditions (Norby et al., 1999; Leakey et al., 2009; Norby and Zak, 2011; Walker et al., 2021). Meta-analysis indicates that stomatal conductance in young trees show stronger response to eCO_2 than old trees, and deciduous forest show stronger response than conifer forest (Medlyn et al., 2001). Furthermore, photosynthesis in C4 plants is close to being saturated, while plants in the C3 carbon pathway are expected to show a greater increase in carbon assimilation rate (Kramer, 1981; Ainsworth and Rogers, 2007; Leakey et al., 2009). Though C4 plants may have more potential response to eCO_2 associated with high WUE (Way et al., 2014). Overall, the uncertain strength of eCO_2 effects across different climate zones and biomes prevents us from better understanding the governing processes, but this is necessary to anticipate future changes of carbon and water fluxes in the system.

This study aims to develop a methodology that would be helpful to define the detectable imprint of CO_2 on land-atmosphere fluxes of carbon and water. Such a detection is challenging with real-world data, mostly due to confounding factors impacting on long-term plant productivity, such as climatic variability, nitrogen

deposition, and land cover change (McCarthy et al., 2010; Schimel et al., 2015; Fernández-Martínez et al., 2017; Liu et al., 2021). FACE experiments provide the opportunities to observe the response of ecosystems to eCO_2 in the field exposed in open-air conditions (Ainsworth and Long, 2005). Nevertheless, in these experiments, ecosystems are pushed into an "accelerating mode" where plants are exposed to a much higher rate of CO_2 concentration increase (≈550 ppm) in a short time period while the climate conditions are changing at a relatively slow speed. Process-based models provide the opportunity to conduct factorial experiments to isolate the role of individual drivers, which allows us to test a statistical trend-detection method. Here, we perform three simulations with the terrestrial biosphere model QUINCY (QUantifying Interactions between terrestrial Nutrient CYcles and the climate system; Thum et al., 2019) to isolate the eCO_2 effects: (i) a reference simulation with transient CO_2 concentrations and observation-based meteorological forcing, (ii) a simulation where the CO_2 is kept constant at the level of 1901 while the meteorological forcing is identical to the reference simulation; and (iii) a simulation with the same set up of (i) but CO_2 is kept constant after the year 1988 at the level of 1988. The simulation (iii) is used to test our method in the recent time period, when the FLUXNET observations start to be recorded. Analyzing the differences of carbon and water fluxes between both simulations, we develop a statistical method to detect the time of emergence of significant eCO_2 effects on these fluxes given their natural variability. In other words, we seek to identify the point in time the eCO_2 effects are distinguishable from short-term and long-term climate effects. We concentrate on the two variables which are most directly affected by rising CO_2, GPP and Tr at annual, seasonal and diurnal scales. To exclude the potential compensation effect of increasing LAI, we normalize Tr by LAI (Tr_{norm}) to obtain the transpiration flux per leaf area. Subsequently, we

analyze eCO_2 effects on ecosystem properties (Table 1) which are important in the carbon and water cycle and investigate controls of the emergence of the eCO_2 effects. We also include Earth system models from the most recent Coupled Model Intercomparison Project (CMIP6) to examine whether the controls of the emergence of the eCO_2 effects are exclusive in the QUINCY model.

2 Materials and Methods

2.1 QUINCY model

2.1.1 Model description

The terrestrial ecosystem model, QUINCY (QUantifying Interactions between terrestrial Nutrient CYcles and the climate system; Thum et al., 2019), is designed to represent the coupled carbon, nitrogen, and phosphorus cycles and their interactions with energy and water balances in terrestrial ecosystems. QUINCY simulates half-hourly carbon, water and energy fluxes as well as longer-term ecosystem dynamics across climate regimes and different plant functional types (PFTs), representing different plant growth forms (tree, grass), leaf types (leaves, needles) and phenology (evergreen, cold and drought deciduous, perennial). Calculation of coupled photosynthesis (Kull and Kruijt, 1998) and stomatal conductance (Medlyn et al., 2011) are taking for sunlit and shaded leaves separately along the vertical canopy gradient of light, foliar chlorophyll and photosynthetic N. QUINCY accounts for limitations of photosynthesis by light, CO_2, temperature and water availability. GPP at the canopy level is integrated from leaf-level gross photosynthesis. The simulated diurnal and seasonal patterns of GPP have been evaluated against a number of benchmarks,

including several FLUXNET sites. Leaf area development is dynamically dependent on plant production (and thereby its response to changing atmospheric CO_2, climate and water availability) as well as stand structural development and turnover through mortality and establishment. Transpiration is calculated as a function of the stomatal conductance of the canopy, aerodynamic conductance, and other parameters in terms of air density and humidity. Soil physics, moisture and biogeochemistry are modelled for 15 layers with exponentially increasing depth. QUINCY calculates the litter and soil organic matter turnover by first-order kinetics with temperature and moisture dependencies. For more detailed explanations of the process representations in QUINCY, please refer to the model description by Thum et al. (2019).

2.1.2 Model setup

2.1.2.1 Boundary conditions and meteorological forcing

The QUINCY model is a 1-D model applied at individual sites (339 sites) distributed across climate zones and biomes for the time period 1901-2018. As an offline land surface model, QUINCY takes time-dependent observation-based meteorological forcing variables as input such as short- and longwave radiation, air temperature, precipitation, vapor pressure deficit (VPD), atmospheric CO_2 concentration, as well as other boundary conditions such as geographical coordinates, PFTs, and soil physical and chemical parameters. At each site, a specific boundary condition and meteorological forcing is taken from the Climate Research Unit and Japanese reanalysis product (CRU JRA V2.1; Harris, 2020), and disaggregated to the model time step (half-hourly) using the statistical weather generator (Zaehle and Friend, 2010). The annual atmospheric CO_2 concentration is obtained from the Global Carbon Project (Le Quéré et al., 2018). Soil physical and chemical properties are derived from

soil texture (Saxton and Rawls, 2006). The texture data are taken from the nearest grid cell of SoilGrids dataset (Hengl et al., 2017). To improve the interpretability of the model simulations with respect to the occurrence of the eCO_2 signal, we reduce the model complexity and set the soil-soluble NH_4, NO_3 and PO_4 concentrations at a prescribed level so that the plant growth is not limited by the nutrient availability, and disregard the N and P deposition in the model.

2.1.2.2 Model simulation experiments for hypothesis testing

We conduct three factorial model experiments to disentangle the effects of eCO_2 from other drivers: (a) Transient-CO_2 experiment. This simulation can be considered as a historical run that aims to approximate the observed system and thus takes the transient climate and CO_2 concentration for the period 1901-2018 as forcing. The transient-CO_2 experiment simulates an increase in atmospheric CO_2 of 110.63 ppm over 118 years; (b) Constant-CO_2 experiment. This simulation includes the same transient climate as the transient-CO_2 experiment. However, the atmospheric CO_2 concentration does not change and is fixed to the initial value of 1901 (296.8 ppm) for the entire simulation period. The climate forcing data contains the effects of rising CO_2. (c) Freeze-CO_2 experiment. Here, the atmospheric CO_2 increases until 1988, as in the transient-CO_2 experiment, but is then kept constant at this value in the years thereafter. The year 1988 was chosen as the time close to the setup of the first FLUXNET sites (Baldocchi et al., 2001).

2.2 Statistical analysis

2.2.1 The effect of elevated CO_2 on annual average GPP and Tr_{norm}

We first calculate the difference in annual average values of GPP and normalized transpiration (Tr_{norm} = Tr / LAI) between the transient-CO_2 and the constant-CO_2 experiments. The difference indicates the eCO_2 effect on the target variable for the period 1901-2018. We cluster the sites based on site-PFT in four vegetation groups: Tropical Forest, Temperate Forest, Boreal Forest and Grasses (Table S1). We further classify the sites of each vegetation group into three temperature classes, “hot”, “warm”, and “cold” based on the quantiles of long-term mean 2m air temperature between the sites in each group. Subdividing the temperature classes further based on the long-term mean annual precipitation (“low”, “middle”, and “high”), we are able to assess the role of water availability in controlling the variability in GPP and normalized transpiration. While the CO_2-induced change of LAI compensates the reduced leaf-level water loss at canopy Tr, it governs GPP in an opposite way. The structural change of increased LAI increases the amount of absorbed photosynthetically active radiation (APAR) and therefore vegetation productivity. We also evaluate the eCO_2 effect on annual average LUE (LUE = GPP / APAR). The part of increased GPP related to increased LAI can be thus disentangled.

2.2.2 Emergence of the elevated CO_2 effects

Based on the CO_2 fertilization effect, we hypothesize that the continuous CO_2 increase over a long period of time exerts a significant influence on the ecosystem (e.g., GPP), which stands out as the eCO_2 effect from natural variability and other factors after a given time and strength of atmospheric CO_2 concentration increase. We define the

emergence of the eCO_2 effects (EoC, ppm) as the change in CO_2 concentration ($\Delta[CO_2]$) required so that the time series of a simulated variable in the transient-CO_2 experiment diverges significantly from the constant-CO_2 experiment. The significant divergence between the two time series is defined by the point in time when the signal exceeds the noise. The noise is intended as the interannual variability of the signal around the long-term changes. We retrieve the signal and noise from the linear fit in the historical time period for each experiment. The calculation of EoC consists of 4 steps: (1) For each site, we calculate annual averages for the target variable (e.g., GPP) from daily model output for both transient-CO_2 and constant-CO_2 experiments for the time period 1901-2018; (2) We apply linear least squares regressions to retrieve the trend in the time series of the target variable from both transient- and constant-CO_2 experiments, respectively, over a given time period (Fig.1). We start with the time period 1901-1910 and iteratively expand this time period year by year by advancing the final year of the time window. For each time period, we compute the linear trend and its uncertainty. Accordingly, we obtain an estimate of the trend and its uncertainties for a total of $n = 108$ points in time for each experiment at each site. The trend b and its standard error $\sigma_b$in the linear regression model are given by (Weisstein, n.d.):

$$b = \frac{\sum_{i=1}^{n}(x_i-\overline{x})(y_i-\overline{y})}{\sum_{i=1}^{n}(x_i-\overline{x})^2}$$

$$\sigma_b = \sqrt{\frac{(\sum_{i=1}^{n}(y_i-\overline{y})^2 - (\sum_{i=1}^{n}(x_i-\overline{x})(y_i-\overline{y}) \times b)/(n-2)}{\sum_{i=1}^{n}(x_i-\overline{x})^2}}$$

Where x is the year at time step i, and y is the value of target variable at the year x_i; (3) The signal is retrieved as the absolute difference in the regression slopes Δb (b in transient-CO_2 minus b in constant-CO_2) as a function of time, while the noise is estimated based on twice the sum of two σ_b from the transient-CO_2 and constant-CO_2

experiments; (4) The time of emergence is determined by the year when the signal exceeds the noise for 5 consecutive years for the first time. The EoC is defined as CO_2 concentration difference ($\Delta[CO_2]$) between the time of emergence and the year 1901 (see Fig. 1 for example). We also test the sensitivity of the arbitrary choice of 5 years in the calculation of EoC and present results also for n (n = 3, 5, 7, 9) years (Fig. S4). For analyzing the freeze-CO_2 experiment we use the same approach to derive the EoC. The only difference is that we set the initial year of keeping CO_2 constant to 1988 instead of 1901.

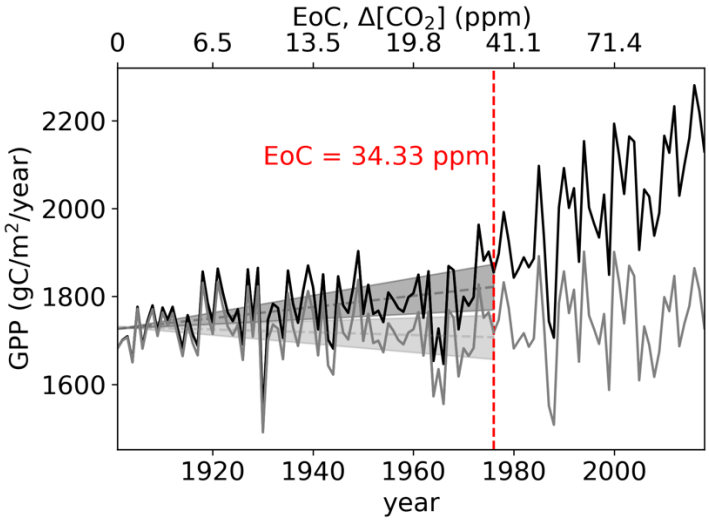

Fig. 1 Illustration of detection of emergence of the elevated CO_2 effects (EoC). The solid lines depict the time series of annual mean GPP for one example site in QUINCY (80.75° W, 37.75° N, temperate broadleaved summer green tree). Black color denotes the time series from the transient-CO_2 experiment, while gray color denotes the time series from the constant-CO_2 experiment (for details see section 2.1.2.2). The shaded area represents the standard error of the linear regression slope (black or gray dashed line). The vertical dashed red line indicates the earliest time at

255 which the black and gray trends deviate significantly. EoC describes the value of

256 $\Delta[CO_2]$ needed to reach this point.

257 **Table 1 Variables and metrics analyzed for the emergence of the elevated CO_2**

258 **effects.**

Variable or metric	Abbreviation
Gross primary production	GPP
Transpiration	Tr
Normalized transpiration per leaf area (Tr/LAI)	Tr_{norm}
Leaf area index	LAI
Net primary production	NPP
Biomass	
Evaporation	
Interception loss	
Root-zone soil moisture	
Light-use efficiency ($GPP/Absorbed\ photosynthetically\ active\ radiation\ (APAR)$)	LUE
Underlying water-use efficiency ($GPP \times \sqrt{VPD}/Tr$)	uWUE
Normalized canopy conductance ($canopy\ conductance\ (gc)/(VPD \times LAI)$)	gc_{norm}
95th percentile of daily GPP values in each year	GPP^{95}
95th percentile of daily Tr_{norm} values in each year	Tr_{norm}^{95}

259

In this study, we mainly focus on the CO_2-induced change on annual average values of the relevant variables and metrics for all sites. Based on existing knowledge, we select variables or metrics (Table 1) that are hypothesized to be most sensitive to eCO_2 (Drake et al., 1997; Novick et al., 2016; Knauer et al., 2017; Ueyama et al., 2020; Migliavacca et al., 2021) to investigate the first manifestations of eCO_2. In addition, to analyze the variation of the CO_2 fertilization effect at different time scales, we apply the same detecting method at specific times-of-day in each year (e.g., 1 May, 8am) instead of annual means, to derive the EoC at seasonal and diurnal scale for representative sites from each vegetation classes (Table S1).

2.2.3 Variable importance determined with random forest analysis

After determining EoC for each site-level simulation, we obtain the respective spatial distribution of EoC across sites. We evaluate the relative contribution from all drivers to the spatial variability in EoC by applying SHapley Additive exPlanation (SHAP) value analysis based on the random forest (RF) model. First, we train the RF model (scikit-learn RandomForestRegressor API in Python, Pedregosa et al., 2011) to predict the previously computed EoC patterns across sites using site-specific long-term (1901-2018) means of climate factors (i.e., temperature, precipitation, soil moisture, VPD, aridity index (evapotranspiration/precipitation)) and vegetation related factors (i.e. GPP, LAI, canopy height, growing season length) as predictors (Fig. S10). The long-term mean values are computed over the entire simulation period from the transient-CO_2 experiment. The out-of-bag (oob) score estimates the accuracy of the prediction from the RF model as compared with the actual EoC values, where a higher

value (the maximum score equals 1) represents a better performance of the model. Finally, we use the module “SHAP TreeExplainer” from the software package shap in Python (Lundberg and Lee, 2017; Lundberg et al., 2020) to examine the influence of all the involved predictors. The average of the absolute SHAP values for each predictor indicates its impact on the target variable (i.e., spatial variability of EoC).

2.3 Comparison with simulations from Earth system models (CMIP6)

In addition, we perform the EoC analysis for GPP and Tr_{norm} using simulations from 7 Earth system models (ESMs) from the most recent Coupled Model Intercomparison Project (CMIP6). We use simulation output of the CMIP6 experiments 1pctCO2 and 1pctCO2-rad. In both experiments, the CO_2 concentration increases gradually at a rate of 1 percent per year until quadrupling, starting at the pre-industrial equilibrium state (Meehl et al., 2014). The fully coupled model setup is used in the 1pctCO2 experiment, while for the 1pctCO2-rad experiment the CO_2 concentration is kept at the pre-industrial level for the carbon cycle and the increasing CO_2 has only a radiative effect (i.e., CO_2-induced climatic changes, Jones et al., 2016). Therefore, the 1pctCO2 experiment is comparable to our transient-CO_2 experiment, and the 1pctCO2-rad experiment is comparable to our constant-CO_2 experiment, although the QUINCY simulations follow the observed CO_2 concentration for the last 120 years. EoC is calculated by applying the same detection method as described in section 2.2.2. To obtain comparability to the EoC results based on the QUINCY simulations, we select cells in gridded CMIP6 output which correspond to the locations of simulated sites with QUINCY. Further, we only consider the CMIP6 time series from the year 1850 until the doubling of the atmospheric CO_2 concentration, i.e., roughly 560 ppm. The ESMs

used in this study are (1) Beijing Climate Center (BCC) BCC-CSM2-MR, (2) Institut Pierre Simon Laplace (IPSL) IPSL-CM6A-LR, (3) Centre National de Recherches Météorologiques (CNRM) CNRM-ESM2-1, (4) United Kingdom (UK) UKESM1-0-LL, (5) Canadian Centre for Climate Modelling and Analysis (CCCma) CanESM5, (6) Meteorological Research Institute of the Japan Meteorological Agency (MRI) MRI-ESM2-0, (7) Max Planck Institute for Meteorology (MPI) MPI-ESM1.2-LR. More details on the used CMIP6 ESMs can be found in (Arora et al., 2020). Due to missing respective output, the analysis for normalized transpiration (Tr_{norm}) only involves the first 4 models in the CMIP6 archive.

3 Results and Discussion

3.1 The effect of elevated CO_2 on gross primary production

Our analysis based on model simulation experiments indicates that eCO_2 generally increases GPP. This increase in GPP differs in magnitude and interannual variability across climate and vegetation types (Fig. 2). The trend of increasing GPP over 118 years is clearly visible in all forested sites and less clear at grassland sites due to high year-to-year variability in GPP. In comparison to the forested sites, the variability in GPP is considerably higher at grassland sites, because grass-dominated ecosystems are more sensitive to climate variability partly related to shallower roots (Kulmatiski et al., 2020; Miguez-Macho and Fan, 2021) and less regulated by stomatal closure (Konings et al., 2017). Grasslands are also predominantly located in semi-arid regions, in which interannual variability of precipitation is large, and therefore has a larger imprint on GPP that it would have in mesic ecosystems with lower precipitation

interannual variability (Maurer et al., 2020). The grassland sites that are located in relatively cold regions show less variability and more clear trends in GPP in contrast to grassland sites located in warmer (and drier) regions.

Overall, the results show that the CO_2 fertilization effect is strong where vegetation productivity is not strongly limited by energy or water availability. Subdividing the temperature classes further based on the amount of annual precipitation, we are able to assess the role of water availability in controlling the variability in GPP (Fig. S2). Sites located in relatively warm and wet regions in the Temperate and the Boreal Forest vegetation class (Fig. S2 b and c) also exhibit the sharpest increase in GPP. This is probably related to the temperature-dependent response of photosynthetic rate of CO_2 uptake through the kinetics of the Rubisco enzyme (Long, 1991; Hickler et al., 2008; Baig et al., 2015). However, the difference of increase in LUE across temperature and precipitation classes are not apparent compared to where we find the sharp increase in GPP, especially in the Temperate Forest vegetation class (Fig. S1 b). The increased carbon assimilation due to rising CO_2 leads to a build-up of more biomass, some of which is allocated to increased leaf growth resulting in an extension of the leaf area (Winkler et al., 2021). Canopies with higher LAI are more available for light interception and therefore it leads to enhancement of vegetation productivity. In temperate forest, the enhancement of GPP due to eCO_2 is the combination of increased both LAI and photosynthetic efficiency (Norby et al., 2005; McCarthy et al., 2006).

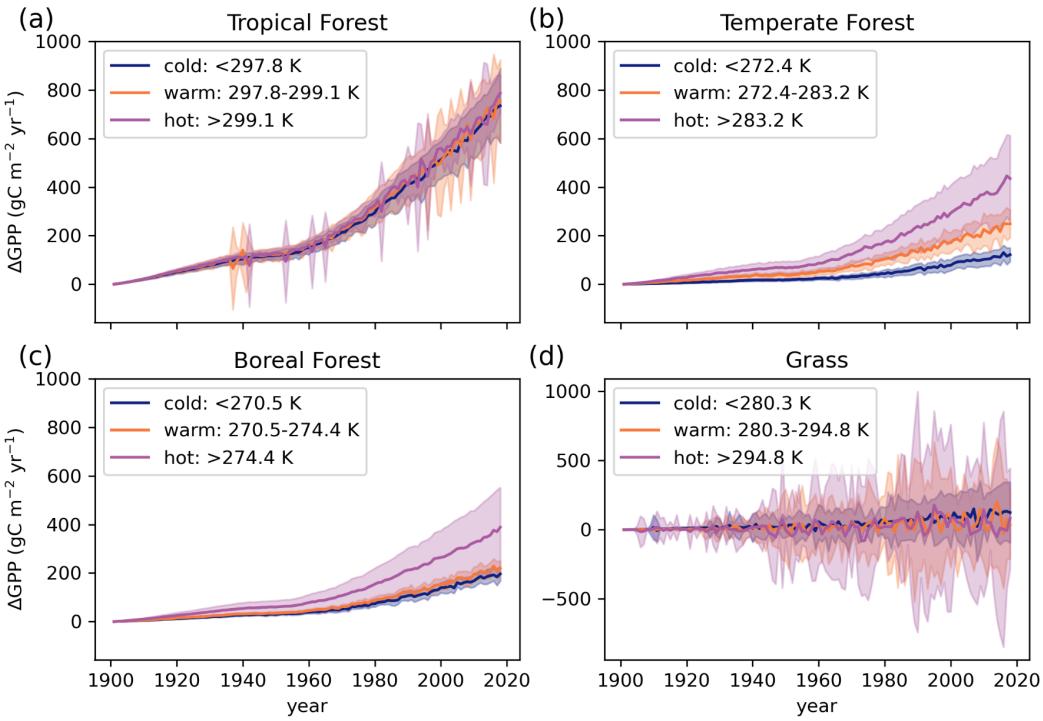

Fig. 2 Differences in annual average GPP between the transient-CO_2 and the constant-CO_2 experiments across climate and vegetation classes. All global sites (339 sites) are first grouped by vegetation type (a-d, Table S1) and then by long-term mean temperature using quantiles within each group (cold in blue: ≤0.33; warm in orange: 0.33 - 0.66; hot in purple: ≥0.66). The shaded area depicts standard deviation around the multi-sites mean value (solid lines).

3.2 The effect of elevated CO_2 on transpiration per leaf area

Decreased transpiration (Tr) due to down-regulated gas exchange with the atmosphere at the leaf level can be offset by an extension in leaf area at the canopy level. The simulated Tr exhibits both increasing and decreasing trends in response to eCO_2. To account for that, we normalized Tr by LAI which is denoted by Tr_{norm}. Tr_{norm} thus represents the transpiration per leaf area.

As expected, we find consistently decreasing Tr_{norm} across all vegetation types and temperature classes (Fig. 3). Similar to the result in section 3.1 (Fig. 2), the variability in Tr_{norm} is high in grasslands. In contrast to GPP, Tr_{norm} responds to eCO_2 strongly where temperature and precipitation are relatively low except for tropical forest sites (Fig. S2). Barton et al. (2012) suggested that the ratio of net photosynthesis to transpiration increases in proportion to the increase in atmospheric CO_2 concentration. They further demonstrated that stomatal conductance responds to eCO_2 not as strongly as the photosynthesis apparatus. At the leaf level, the decreased stomatal conductance is likely to result in the increase of leaf skin temperature (Leakey et al., 2009), which demands higher transpiration. However, the direct relationship between ambient temperature and eCO_2 effect on stomatal regulation is still ambiguous (Medlyn et al., 2001; Barton et al., 2012).

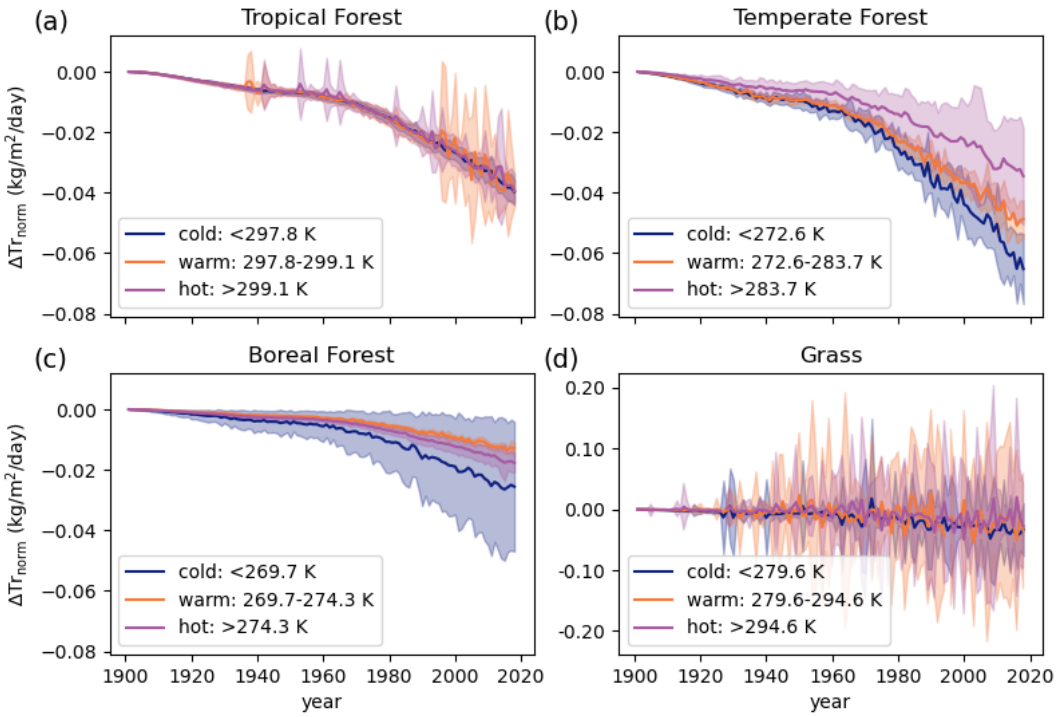

Fig. 3 Differences in annual average Tr_{norm} between the transient-CO_2 and the constant-CO_2 experiments across climate and vegetation classes. All global sites

(339 sites) are first grouped by vegetation type (a-d, Table S1) and then by temperature using quantiles (cold in blue: ≤0.33; warm in orange: 0.33 - 0.66; hot in purple: ≥0.66). The shaded area depicts standard deviation around the multi-sites mean value (solid lines).

3.3 Emergence of the elevated CO_2 effects (EoC) in GPP and Tr_{norm}

A lower EoC indicates a detection of eCO_2 effects earlier in the analyzed time period and thus a stronger response in the target variable to the eCO_2 effects compared to its background or natural variability. Our results show that the eCO_2 effect in GPP is strongest in the tropical forests. 44 sites exhibit an EoC of less than 20 ppm (Fig. 4). This means that a change in atmospheric CO_2 of 20 ppm is sufficient to detect the CO_2 fertilization effect in the GPP time series for those sites. The forested northern mid- and high-latitudes also exhibit significant changes in GPP, which, however, is only detectable at much higher $\Delta[CO_2]$ (consistent with Schimel et al., 2015). GPP in arid regions is highly variable due to the high sensitivity towards intermittent water availability, and this prevents a detection of the CO_2 fertilization effect. The effect of eCO_2 on GPP further rarely emerges in regions dominated by C4 grasses, most likely because they are less responsive to eCO_2 due to their different photosynthetic pathway (Leakey et al., 2009). Also, evidence from FACE experiments suggests that trees exhibit the greatest response to eCO_2 compared to C3 and C4 grasses (Ainsworth and Long, 2005). The magnitude of plants' responses to eCO_2 comes down to the variations of photosynthetic capacity, which is indicated by the maximum rate of

399 RuBisCO carboxylase activity (Vc_{max}) and the maximum rate of photosynthetic
400 electron transport (J_{max}; Long, 1991). We find a similar pattern of distribution for EoC
401 in LUE (Fig. S5) with EoC in GPP, which could support the physiological effect of eCO_2
402 on GPP rather than structural change, namely the change of LAI.
403 EoC in Tr_{norm} is substantially higher compared to GPP, i.e., the signal emerges only at
404 considerably higher $\Delta[CO_2]$. Further, the global spatial pattern of EoC is more
405 homogeneous for Tr_{norm} than for GPP. Several equatorial sites exhibit a relatively low
406 EoC (some of them even less than 40 ppm), but for most sites (123 in 152 detected
407 sites) the signal only emerges at $\Delta[CO_2] > 70$ ppm or not at all. Especially at sites in
408 arid and semi-arid regions, no significant effect of eCO_2 can be detected, even though
409 a strong response in water-use efficiency is expected to occur in these water-limited
410 ecosystems (Medlyn et al., 2001). In the QUINCY model, canopy conductance and
411 transpiration does not scale linearly with LAI at canopy level. So, the Tr_{norm} could still
412 be affected by increasing LAI to some extent. Next to this, transpiration can be affected
413 by other factors which may overshadow the role of stomatal conductance. For
414 example, transpiration is affected by incoming radiation particularly when vegetation
415 is strongly decoupled with the boundary layer, i.e., a low exchange rate between
416 vegetation and atmosphere (Jarvis, 1985; De Kauwe et al., 2017). Due to the limited
417 representation of the coupling between vegetation and the boundary layer in models,
418 the reduced transpiration flux at the leaf-level might not scale to the canopy-level.
419 The freeze-CO_2 experiment (see section 2.1.2.2) reveals if the results are still
420 informative for climate change in recent years (1988-2018). Due to the limited length
421 of the time period, there are only a few sites where the eCO_2 effect on GPP can be

detected (Fig. S6). Nevertheless, as the result shown in Fig. 4a, the signal first emerges in the tropical regions, with a rather low EoC of around 20 ppm. Furthermore, the EoC for tropical GPP is consistent between two time periods (1901-2018 and 1988-2018). This encourages future study of the CO_2 fertilization effect in recent years.

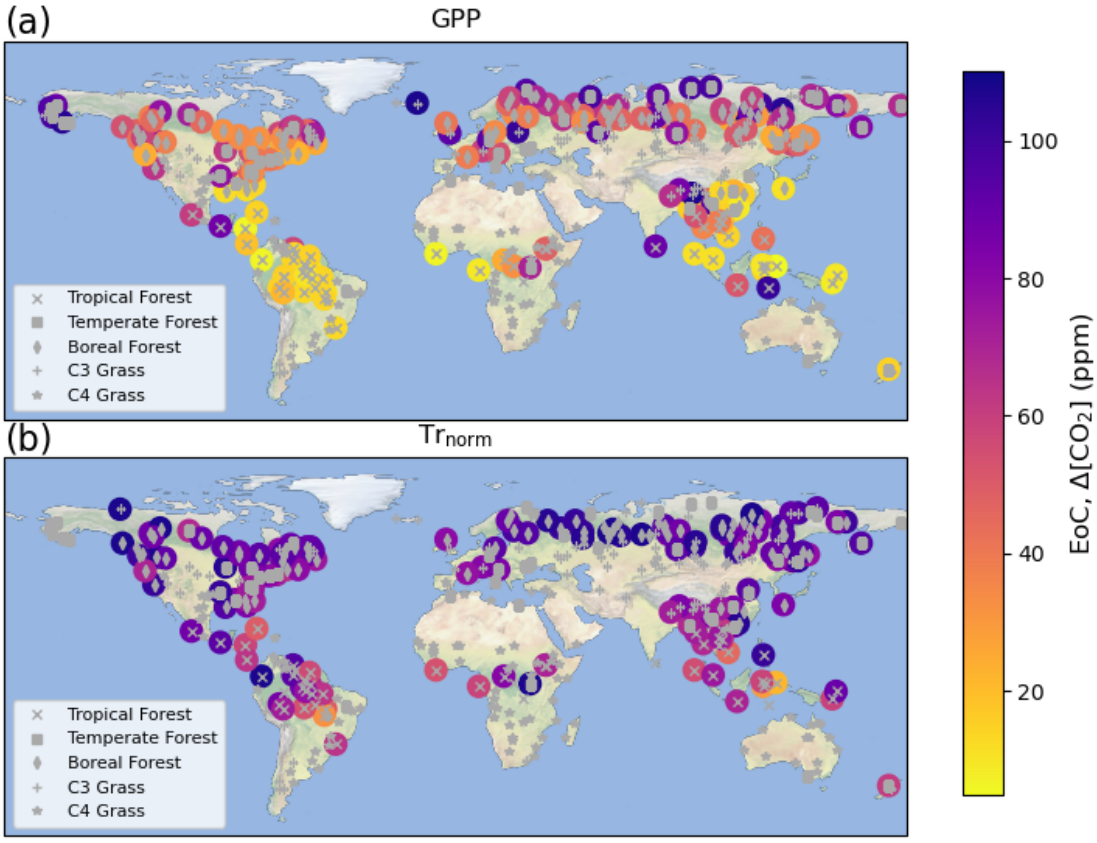

Fig. 4 Global distribution of emergence of the elevated CO_2 effects (EoC) in (a) GPP and (b) Tr_{norm}. Bright color indicates an earlier detection (lower EoC), and dark color indicates a later detection (higher EoC). Non-colored points indicate sites where the elevated CO_2 does not translate into significant changes in GPP or Tr_{norm} within the historical time period.

3.4 Seasonal and diurnal variation of EoC in GPP

We find plants respond differently to the effects of eCO_2 across different climate zones and vegetation types, but also in different seasons and times of the day. For example, EoC in GPP is lower in summer than in other seasons at sites in the temperate and boreal forests (Fig. S7 a, d), which is obviously driven by favorable growing conditions. However, this is not always the case at the diurnal time scale where lowest EoC are partly found at other times than noon. For the sites in temperate and boreal forests, the strong signal already emerges early in the morning on some days during summer. It could be related to the increased aridity at midday. The excessive atmospheric moisture demand at high temperature results in the midday depression of carbon uptake, and thus stomatal limitation, which can be simulated by the model. Unlike for the boreal forest site, at the tropical forest site (Fig. S7 b), the plant response to eCO_2 can be detected for any time during the daytime and in all seasons. Although the effect of eCO_2 on GPP cannot be detected at grass sites at the annual scale, we can detect it in the early growing season, albeit only at very high $\Delta[CO_2]$ > ~100 ppm (Fig. 3, Fig. S7 c). The EoC in Tr_{norm} however is not detectable at any point of the the seasonal and diurnal cycle, probably related to high variability of the meteorological conditions, which can be reduced to some extent by the aggregation to annual values. In the future, researchers may explore the drivers of the variation across diurnal and seasonal scales. Furthermore, we find the EoC in GPP is lower at some points of the seasonal and diurnal cycle than EoC in GPP at the annual scale (Fig. S7). This motivates future study of eCO_2 effects in observations at the seasonal and diurnal time scale.

3.5 EoC in secondary variables triggered by plant physiological effects

Changes in GPP and Tr_{norm} triggered by the effects of eCO_2 can cascade into secondary state and process variables of the carbon (e.g., LAI, biomass, NPP) and water cycles (e.g., evaporation, interception loss, soil moisture). The EoC in LAI and biomass are generally low (Fig. S8 a, b), even lower than in the case of GPP. Note that this does not mean that LAI responds more strongly to CO_2 increases than GPP, but rather this finding illustrates the effect of the internal variabilities of each variable on our results where LAI and biomass as state variables are less influenced by short-term and interannual hydro-meteorological variations and therefore its variation has a substantially lower standard deviation. The higher signal-to-noise ratio enables the detection of the eCO_2 effects already early in the time series where CO_2 has not yet increased much. Additionally, there is a non-linear relationship between GPP and LAI when LAI is high. GPP tends to saturate with high LAI due to clumping and the increase of shaded leaves in the canopy (Street et al., 2007; Chen et al., 2012; Lee et al., 2019). However, except for the eCO_2 effect, different carbon allocation representations in models also affect the prediction for where the additionally assimilated carbon goes (Kauwe et al., 2014). Further, the modeled carbon pathways do not always agree with observational evidence from elevated CO_2 experiments (Norby and Zak, 2011). EoC in NPP shows a similar spatial pattern compared to EoC in GPP, only the EoC is overall higher due to the added variability from autotrophic respiration (Fig. S8 c).

The natural variability of process and state variables in the water cycle (e.g., evaporation, interception, root-zone soil moisture) is substantially higher than for the

carbon cycle variables. The increasing LAI could provide more shading area, resulting in a cooling of the surface soil layer. The evaporation from bare soil decreases as a consequence of this reduced radiative energy input. Consequently, the EoC in evaporation can be detected in sites located mainly in tropical regions and mid-latitude regions (Fig. S8 d). Evaporation from rainfall interception is expected to remarkably increase due to the substantial increase in LAI. However, the magnitude of increased interception loss does not stand out from the year-to-year variability controlled by stochastic precipitation events. Also, the root-zone soil moisture does not exhibit a clear response to eCO_2. This is related to the complex and interacting effects on related water fluxes such as soil evaporation, transpiration, interception loss and runoff. The interannual variability in precipitation likely also overshadows the subtle changes in soil moisture in response to the effects of eCO_2 (De Kauwe et al., 2021).

3.6 First manifestations of elevated CO_2

In this section we compare the EoC across several variables and metrics (Table 1) related to the carbon and water cycles. These variables and metrics include the underlying water-use efficiency (uWUE), the light-use efficiency (LUE), the normalized canopy conductance (gc_{norm}), LAI and the 95th percentiles of GPP (GPP^{95}) and Tr_{norm} (Tr_{norm}^{95}). EoC is lowest for GPP^{95} and LAI for most sites (167 in 214 detected sites; Fig. 5). We consider the 95th percentile of daily GPP values in each year (GPP^{95}) to be representative of the maximum capacity of vegetation productivity, which is less affected by day-to-day weather variability. EoC in GPP^{95} is significantly lower since much of the variability is removed compared to annual mean GPP. EoC in GPP^{95} and LAI are comparable in the vegetation classes Tropical and Boreal Forests (Fig. S9). However, EoC in LAI in the Temperate Forests and Grass vegetation classes tends to

be considerably higher. Probably, this is due to the different fraction of carbon allocated to foliage versus other plant components across vegetation types (De Kauwe et al., 2014).

EoC in LUE emerges first for sites located in the high latitudinal regions, where plant growth is considered to be energy-limited. EoC in WUE emerges first for sites in arid regions, where plant growth is limited by water availability. Compared to variables related to the carbon cycle (e.g., GPP, GPP^{95}, LAI), variables related to the water cycle (e.g., gc_{norm}, Tr_{norm}, Tr_{norm}^{95}) show weaker responses to the physiological effects of eCO_2.

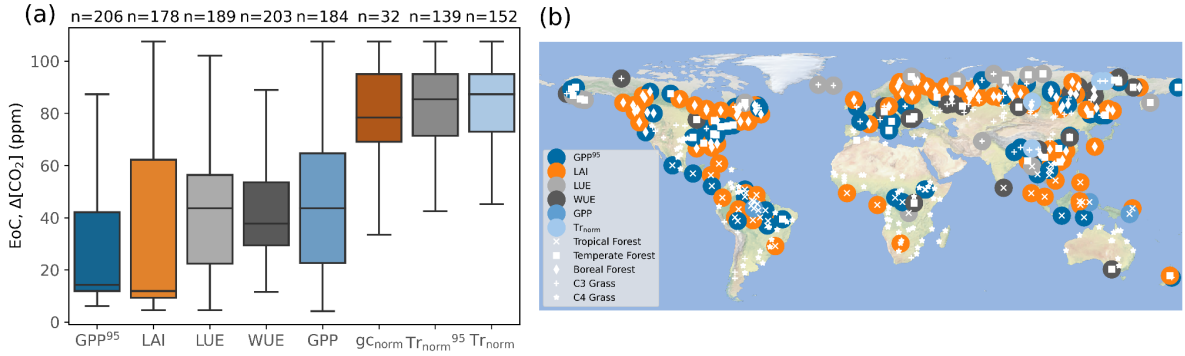

Fig. 5 Comparison of EoC across variables and metrics. (a) Box plots depict the GPP, 95th percentile of daily GPP values in each year (GPP^{95}), LAI, light-use efficiency (LUE), underlying water-use efficiency (uWUE), gc_{norm}, Tr_{norm}, 95th percentile of daily Tr_{norm} values in each year (Tr_{norm}^{95}). Box plots indicate medians and inter-quantile ranges, and are ordered according to the mean EoC across sites for each variable. Numbers above the boxplots indicate how many sites can be detected for each variable or metric (339 sites in total). (b) The map shows the first-emerging variable or metric with the lowest EoC. The white points on the map refer to the geographical locations of all sites.

3.7 Explaining the spatial variability of EoC in GPP and Tr_{norm}

The ecosystem responses to eCO_2 are complex and modulated by several concurrent effects. All drivers considered to explain the spatial variability of EoC are calculated as long-term mean values (see section 2.2.3). We find that the spatial variability of EoC in GPP and Tr_{norm} between sites is mainly explained by varying levels of mean LAI and mean GPP, respectively (Fig. S10). The higher the mean LAI (or mean GPP), the less $\Delta[CO_2]$ is required such that the physiological effects of eCO_2 emerge in GPP, respectively, Tr_{norm} fluxes. Next, we compare these relationships based on the QUINCY model with output from similar simulations of Earth system models conducted in CMIP6 (see section 2.3). Most CMIP6 models qualitatively agree with the QUINCY results, i.e., the negative relationship between spatial EoC in GPP and LAI, and the negative relationship between spatial EoC in Tr_{norm} and GPP (Fig. 6). Four models in CMIP6 (Fig. S11 (a)(e)(f)(g)) agree with QUINCY (Fig. S11 (h)), while the other three of them do not show a negative relationship between EoC in GPP and the long-term mean LAI. Also, there are considerable differences between the magnitude of EoC across the models as well as the strength of the relationships vary among the individual models in CMIP6 (Fig. S11, Fig. S12). We note, however, that this direct comparison between the QUINCY and the CMIP6 simulations is limited due to the conceptually different setup of the analysed simulations. Furthermore, in contrast to the QUINCY model, which is an offline terrestrial biosphere point model, the CMIP6 ensemble comprises fully coupled Earth system models, which represent a gridded and coupled land-atmosphere system. Despite these conceptual differences, the

overall agreement between the QUINCY and CMIP6 models illustrated in Fig. 6 corroborates our findings based on the QUINCY model formulation.

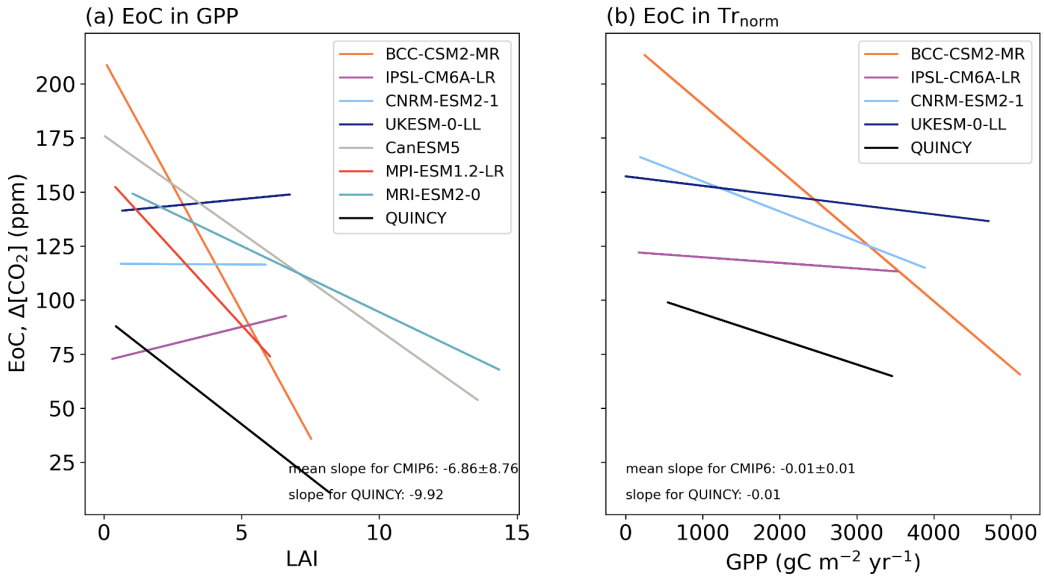

Fig. 6 EoC in QUINCY versus coupled Earth system models. Spatially varying EoC is plotted against the predictor that explains most of its spatial variability according to the SHAP value analysis illustrated in Fig. S10. The relationship of (a) EoC in GPP is plotted against respective LAI of each model; and (b) EoC in Tr_{norm} is plotted against respective baseline GPP from each model.

4 Conclusion

We evaluate the plant physiological effects of elevated CO_2 (eCO_2) on the land-atmosphere exchange of carbon and water. Increasing atmospheric CO_2 stimulates plant carbon assimilation and reduces stomatal conductance, which both may result in a potential increase in ecosystem productivity and also affect ecosystem transpiration. Analyzing approximately the last 120 years simulated by the terrestrial biosphere model QUINCY, we assess how strong the increase in CO_2 needs to be

such that the effects of eCO_2 surpass the noise and effects induced by short and long-term meteorological conditions.

We find that the eCO_2 effects on GPP can be earlier detected compared with transpiration (Tr). The eCO_2 effects on GPP are different across climate and biomes, whereas eCO_2 effects on normalized transpiration (Tr_{norm}) exhibit less spatial variability. The eCO_2 effects on GPP are detectable at relatively low CO_2 increase ($\Delta[CO_2] \sim 20$ ppm) in regions where vegetation productivity is not strongly constrained by climatic conditions, i.e., water- or temperature-limited plant growth. Carbon assimilation and carbon pools show stronger responses to eCO_2 across sites while we do not find a widespread strong eCO_2 effect in variables describing the water cycle. The transpiration at canopy level is regulated by the reduced stomatal conductance and meanwhile, the increasing LAI in response to eCO_2. These two opposing effects appear to be cancelled each other out at ecosystem level and longer time scales, resulting in an insignificant eCO_2 effect on transpiration and other water cycle variables (e.g., evaporation, interception loss and soil moisture) which are affected by the response of Tr. While mostly GPP and LAI are the first variables to exhibit detectable eCO_2 effects, in northern high-latitude regions where vegetation growth is limited by radiation, light-use efficiency responds to eCO_2 first among all the other variables, and the eCO_2 effects on water-use efficiency emerges first in some sites located in semi-arid regions.

Climate variations can partly explain the spatial heterogeneity of the plant physiological effects of eCO_2. The strongest response of GPP or Tr_{norm} to eCO_2 occurs dominantly where GPP is not limited by either temperature or precipitation (e.g., sites in tropical regions). The weakest response of GPP or Tr_{norm} occurs in arid regions

585 (e.g., grassland sites), where the high variability overshadows the eCO_2 effect. In
586 addition to climate factors, eCO_2-induced plant physiological effects are amplified
587 where vegetation productivity is already high. We find the long-term mean LAI is the
588 dominant driver of spatial variability of the eCO_2 effect on GPP, whereas the long-term
589 mean GPP is the dominant driver of spatial variability of the eCO_2 effect on Tr_{norm}.
590 Despite the different model structures and simulation setups, the CMIP6 models
591 essentially are consistent with the insights gained from the QUINCY model about what
592 drives spatial variance in the emergence of the eCO_2 effects. Overall, our results thus
593 suggest that high-LAI regions, e.g., tree-dominated ecosystems are more sensitive to
594 the eCO_2 effect than low-LAI, e.g., grass-dominated ecosystems.
595 Models have the advantage for hypothesis testing by conducting idealized
596 experiments. Using these experiments, we determine when and where we expect to
597 detect the eCO_2 effects according to our theoretical understanding formulated in the
598 models. This knowledge provides a first step towards assessing long-term changes
599 and trends in carbon and water flux observations using eddy covariance
600 measurements (Baldocchi et al., 2001). In a future study, we will apply this
601 methodology to analyze whether eCO_2 effects can already be detected in the time
602 series of long-term measurement campaigns of land-atmosphere exchange fluxes,
603 focusing on the regions and time scales of eCO_2 effects spotlighted in this precursory
604 study. Overall, the model-based analyses presented here, along with the ongoing
605 observational study focused on the detection and potential quantification of eCO_2
606 effects, are critical and have long been called for in order to provide robust
607 assessments of how the system will continue to change as CO_2 continues to rise.

Acknowledgements

Chunhui Zhan is supported by the International Max Planck Research School (IMPRS). Markus Reichstein and Alexander J. Winkler acknowledge support by the European Research Council (ERC) Synergy Grant “Understanding and Modelling the Earth System with Machine Learning (USMILE)” under the Horizon 2020 research and innovation programme (Grant agreement No. 855187). René Orth is supported by the German Research Foundation (Emmy Noether grant number 391059971). Sönke Zaehle and Jan Engel were supported by the European Research Council (ERC) under the European Union's Horizon 2020 research and innovation programme (QUINCY; grant no. 647204). Chunhui Zhan thanks Silvia Caldararu and Lin Yu for their support in working with the QUINCY model.

Author contributions

Chunhui Zhan, Rene Orth and Alexander J. Winkler jointly designed this study. Mirco Migliavacca, Sönke Zaehle and Markus Reichstein contributed to ideas and experimental design. Alexander J. Winkler preprocessed the CMIP6 model simulations. Jan Engel contributed to technical assistance for the QUINCY model. All authors contributed to the writing of the paper, the discussion and interpretation of the results.

Competing interests

The authors declare that there are no competing interests.

References

Ainsworth, E.A., Long, S.P., 2005. What have we learned from 15 years of free-air CO2 enrichment (FACE)? A meta-analytic review of the responses of photosynthesis,

canopy properties and plant production to rising CO2. New Phytol. 165, 351–372. https://doi.org/10.1111/j.1469-8137.2004.01224.x

Ainsworth, E.A., Rogers, A., 2007. The response of photosynthesis and stomatal conductance to rising [CO2]: mechanisms and environmental interactions. Plant Cell Environ. 30, 258–270. https://doi.org/10.1111/j.1365-3040.2007.01641.x

Arora, V.K., Katavouta, A., Williams, R.G., Jones, C.D., Brovkin, V., Friedlingstein, P., Schwinger, J., Bopp, L., Boucher, O., Cadule, P., Chamberlain, M.A., Christian, J.R., Delire, C., Fisher, R.A., Hajima, T., Ilyina, T., Joetzjer, E., Kawamiya, M., Koven, C.D., Krasting, J.P., Law, R.M., Lawrence, D.M., Lenton, A., Lindsay, K., Pongratz, J., Raddatz, T., Séférian, R., Tachiiri, K., Tjiputra, J.F., Wiltshire, A., Wu, T., Ziehn, T., 2020. Carbon–concentration and carbon–climate feedbacks in CMIP6 models and their comparison to CMIP5 models. Biogeosciences 17, 4173–4222. https://doi.org/10.5194/bg-17-4173-2020

Baig, S., Medlyn, B.E., Mercado, L.M., Zaehle, S., 2015. Does the growth response of woody plants to elevated CO2 increase with temperature? A model-oriented meta-analysis. Glob. Change Biol. 21, 4303–4319. https://doi.org/10.1111/gcb.12962

Baldocchi, D., Falge, E., Gu, L., Olson, R., Hollinger, D., Running, S., Anthoni, P., Bernhofer, C., Davis, K., Evans, R., Fuentes, J., Goldstein, A., Katul, G., Law, B., Lee, X., Malhi, Y., Meyers, T., Munger, W., Oechel, W., U, K.T.P., Pilegaard, K., Schmid, H.P., Valentini, R., Verma, S., Vesala, T., Wilson, K., Wofsy, S., 2001. FLUXNET: A New Tool to Study the Temporal and Spatial Variability of Ecosystem-Scale Carbon Dioxide, Water Vapor, and Energy Flux Densities. Bull. Am. Meteorol. Soc. 82, 2415–2434. https://doi.org/10.1175/1520-0477(2001)082<2415:FANTTS>2.3.CO;2

Barton, C.V.M., Duursma, R.A., Medlyn, B.E., Ellsworth, D.S., Eamus, D., Tissue, D.T., Adams, M.A., Conroy, J., Crous, K.Y., Liberloo, M., Löw, M., Linder, S., McMurtrie, R.E., 2012. Effects of elevated atmospheric [CO2] on instantaneous transpiration efficiency at leaf and canopy scales in Eucalyptus saligna. Glob. Change Biol. 18, 585–595. https://doi.org/10.1111/j.1365-2486.2011.02526.x

Bastos, A., Ciais, P., Friedlingstein, P., Sitch, S., Pongratz, J., Fan, L., Wigneron, J.P., Weber, U., Reichstein, M., Fu, Z., Anthoni, P., Arneth, A., Haverd, V., Jain, A.K., Joetzjer, E., Knauer, J., Lienert, S., Loughran, T., McGuire, P.C., Tian, H., Viovy, N., Zaehle, S., 2020. Direct and seasonal legacy effects of the 2018 heat wave and drought on European ecosystem productivity. Sci. Adv. https://doi.org/10.1126/sciadv.aba2724

Chen, J.M., Mo, G., Pisek, J., Liu, J., Deng, F., Ishizawa, M., Chan, D., 2012. Effects of foliage clumping on the estimation of global terrestrial gross primary productivity. Glob. Biogeochem. Cycles 26. https://doi.org/10.1029/2010GB003996

De Kauwe, M.G., Medlyn, B.E., Knauer, J., Williams, C.A., 2017. Ideas and perspectives: how coupled is the vegetation to the boundary layer? Biogeosciences 14, 4435–4453. https://doi.org/10.5194/bg-14-4435-2017

De Kauwe, M.G., Medlyn, B.E., Tissue, D.T., 2021. To what extent can rising [CO2] ameliorate plant drought stress? New Phytol. 231, 2118–2124. https://doi.org/10.1111/nph.17540

Drake, B.G., Gonzàlez-Meler, M.A., Long, S.P., 1997. MORE EFFICIENT PLANTS: A Consequence of Rising Atmospheric CO2? Annu. Rev. Plant Physiol. Plant Mol. Biol. 48, 609–639. https://doi.org/10.1146/annurev.arplant.48.1.609

Fernández-Martínez, M., Vicca, S., Janssens, I.A., Ciais, P., Obersteiner, M., Bartrons, M., Sardans, J., Verger, A., Canadell, J.G., Chevallier, F., Wang, X., Bernhofer, C., Curtis, P.S., Gianelle, D., Grünwald, T., Heinesch, B., Ibrom, A., Knohl, A., Laurila, T., Law, B.E., Limousin, J.M., Longdoz, B., Loustau, D., Mammarella, I., Matteucci, G., Monson, R.K., Montagnani, L., Moors, E.J., Munger, J.W., Papale, D., Piao, S.L., Peñuelas, J., 2017. Atmospheric deposition, CO 2 , and change in the land carbon sink. Sci. Rep. 7, 9632. https://doi.org/10.1038/s41598-017-08755-8

Friedlingstein, P., Jones, M.W., O'Sullivan, M., Andrew, R.M., Hauck, J., Peters, G.P., Peters, W., Pongratz, J., Sitch, S., Le Quéré, C., Bakker, D.C.E., Canadell, J.G., Ciais, P., Jackson, R.B., Anthoni, P., Barbero, L., Bastos, A., Bastrikov, V., Becker,

685 M., Bopp, L., Buitenhuis, E., Chandra, N., Chevallier, F., Chini, L.P., Currie, K.I.,
686 Feely, R.A., Gehlen, M., Gilfillan, D., Gkritzalis, T., Goll, D.S., Gruber, N., Gutekunst,
687 S., Harris, I., Haverd, V., Houghton, R.A., Hurtt, G., Ilyina, T., Jain, A.K., Joetzjer, E.,
688 Kaplan, J.O., Kato, E., Klein Goldewijk, K., Korsbakken, J.I., Landschützer, P.,
689 Lauvset, S.K., Lefèvre, N., Lenton, A., Lienert, S., Lombardozzi, D., Marland, G.,
690 McGuire, P.C., Melton, J.R., Metzl, N., Munro, D.R., Nabel, J.E.M.S., Nakaoka, S.-I.,
691 Neill, C., Omar, A.M., Ono, T., Peregon, A., Pierrot, D., Poulter, B., Rehder, G.,
692 Resplandy, L., Robertson, E., Rödenbeck, C., Séférian, R., Schwinger, J., Smith, N.,
693 Tans, P.P., Tian, H., Tilbrook, B., Tubiello, F.N., van der Werf, G.R., Wiltshire, A.J.,
694 Zaehle, S., 2019. Global Carbon Budget 2019. Earth Syst. Sci. Data 11, 1783–1838.
695 https://doi.org/10.5194/essd-11-1783-2019
696 Gedney, N., Cox, P.M., Betts, R.A., Boucher, O., Huntingford, C., Stott, P.A., 2006.
697 Detection of a direct carbon dioxide effect in continental river runoff records. Nature
698 439, 835–838. https://doi.org/10.1038/nature04504
699 Gentine, P., Green, J.K., Guérin, M., Humphrey, V., Seneviratne, S.I., Zhang, Y., Zhou, S.,
700 2019. Coupling between the terrestrial carbon and water cycles—a review. Environ.
701 Res. Lett. 14, 083003. https://doi.org/10.1088/1748-9326/ab22d6
702 Good, S.P., Noone, D., Bowen, G., 2015. Hydrologic connectivity constrains partitioning of
703 global terrestrial water fluxes. Science 349, 175–177.
704 https://doi.org/10.1126/science.aaa5931
705 Hengl, T., Jesus, J.M. de, Heuvelink, G.B.M., Gonzalez, M.R., Kilibarda, M., Blagotić, A.,
706 Shangguan, W., Wright, M.N., Geng, X., Bauer-Marschallinger, B., Guevara, M.A.,
707 Vargas, R., MacMillan, R.A., Batjes, N.H., Leenaars, J.G.B., Ribeiro, E., Wheeler, I.,
708 Mantel, S., Kempen, B., 2017. SoilGrids250m: Global gridded soil information based
709 on machine learning. PLOS ONE 12, e0169748.
710 https://doi.org/10.1371/journal.pone.0169748
711 Hickler, T., Smith, B., Prentice, I.C., Mjöfors, K., Miller, P., Arneth, A., Sykes, M.T., 2008.
712 CO2 fertilization in temperate FACE experiments not representative of boreal and

713 tropical forests. Glob. Change Biol. 14, 1531–1542. https://doi.org/10.1111/j.1365-
714 2486.2008.01598.x
715 Jarvis, P.G., 1985. Transpiration and assimilation of tree and agricultural crops: the “omega
716 factor.” Attrib. Trees Crop Plants Ed. MGR Cannell JE Jackson.
717 Jones, C.D., Arora, V., Friedlingstein, P., Bopp, L., Brovkin, V., Dunne, J., Graven, H.,
718 Hoffman, F., Ilyina, T., John, J.G., Jung, M., Kawamiya, M., Koven, C., Pongratz, J.,
719 Raddatz, T., Randerson, J.T., Zaehle, S., 2016. C4MIP – The Coupled
720 Climate–Carbon Cycle Model Intercomparison Project: experimental protocol for
721 CMIP6. Geosci. Model Dev. 9, 2853–2880. https://doi.org/10.5194/gmd-9-2853-2016
722 Kauwe, M.G.D., Medlyn, B.E., Zaehle, S., Walker, A.P., Dietze, M.C., Wang, Y.-P., Luo, Y.,
723 Jain, A.K., El-Masri, B., Hickler, T., Wårlind, D., Weng, E., Parton, W.J., Thornton,
724 P.E., Wang, S., Prentice, I.C., Asao, S., Smith, B., McCarthy, H.R., Iversen, C.M.,
725 Hanson, P.J., Warren, J.M., Oren, R., Norby, R.J., 2014. Where does the carbon go?
726 A model–data intercomparison of vegetation carbon allocation and turnover
727 processes at two temperate forest free-air CO2 enrichment sites. New Phytol. 203,
728 883–899. https://doi.org/10.1111/nph.12847
729 Keenan, T.F., Hollinger, D.Y., Bohrer, G., Dragoni, D., Munger, J.W., Schmid, H.P.,
730 Richardson, A.D., 2013. Increase in forest water-use efficiency as atmospheric
731 carbon dioxide concentrations rise. Nature 499, 324–327.
732 https://doi.org/10.1038/nature12291
733 Knauer, J., Zaehle, S., Reichstein, M., Medlyn, B.E., Forkel, M., Hagemann, S., Werner, C.,
734 2017. The response of ecosystem water-use efficiency to rising atmospheric CO_2
735 concentrations: sensitivity and large-scale biogeochemical implications. New Phytol.
736 213, 1654–1666. https://doi.org/10.1111/nph.14288
737 Konings, A.G., Williams, A.P., Gentine, P., 2017. Sensitivity of grassland productivity to
738 aridity controlled by stomatal and xylem regulation. Nat. Geosci. 10, 284–288.
739 https://doi.org/10.1038/ngeo2903

Körner, C., Morgan, J., Norby, R., 2007. CO2 Fertilization: When, Where, How Much?, in: Canadell, J.G., Pataki, D.E., Pitelka, L.F. (Eds.), Terrestrial Ecosystems in a Changing World, Global Change — The IGBP Series. Springer, Berlin, Heidelberg, pp. 9–21. https://doi.org/10.1007/978-3-540-32730-1_2

Kramer, P.J., 1981. Carbon Dioxide Concentration, Photosynthesis, and Dry Matter Production. BioScience 31, 29–33. https://doi.org/10.2307/1308175

Kull, O., Kruijt, B., 1998. Leaf photosynthetic light response: a mechanistic model for scaling photosynthesis to leaves and canopies. Funct. Ecol. 12, 767–777. https://doi.org/10.1046/j.1365-2435.1998.00257.x

Kulmatiski, A., Adler, P.B., Foley, K.M., 2020. Hydrologic niches explain species coexistence and abundance in a shrub–steppe system. J. Ecol. 108, 998–1008. https://doi.org/10.1111/1365-2745.13324

Le Quéré, C., Andrew, R.M., Friedlingstein, P., Sitch, S., Pongratz, J., Manning, A.C., Korsbakken, J.I., Peters, G.P., Canadell, J.G., Jackson, R.B., Boden, T.A., Tans, P.P., Andrews, O.D., Arora, V.K., Bakker, D.C.E., Barbero, L., Becker, M., Betts, R.A., Bopp, L., Chevallier, F., Chini, L.P., Ciais, P., Cosca, C.E., Cross, J., Currie, K., Gasser, T., Harris, I., Hauck, J., Haverd, V., Houghton, R.A., Hunt, C.W., Hurtt, G., Ilyina, T., Jain, A.K., Kato, E., Kautz, M., Keeling, R.F., Klein Goldewijk, K., Körtzinger, A., Landschützer, P., Lefèvre, N., Lenton, A., Lienert, S., Lima, I., Lombardozzi, D., Metzl, N., Millero, F., Monteiro, P.M.S., Munro, D.R., Nabel, J.E.M.S., Nakaoka, S., Nojiri, Y., Padin, X.A., Peregon, A., Pfeil, B., Pierrot, D., Poulter, B., Rehder, G., Reimer, J., Rödenbeck, C., Schwinger, J., Séférian, R., Skjelvan, I., Stocker, B.D., Tian, H., Tilbrook, B., Tubiello, F.N., van der Laan-Luijkx, I.T., van der Werf, G.R., van Heuven, S., Viovy, N., Vuichard, N., Walker, A.P., Watson, A.J., Wiltshire, A.J., Zaehle, S., Zhu, D., 2018. Global Carbon Budget 2017. Earth Syst. Sci. Data 10, 405–448. https://doi.org/10.5194/essd-10-405-2018

Leakey, A.D.B., Ainsworth, E.A., Bernacchi, C.J., Rogers, A., Long, S.P., Ort, D.R., 2009. Elevated CO2 effects on plant carbon, nitrogen, and water relations: six important

768 lessons from FACE. J. Exp. Bot. 60, 2859–2876. https://doi.org/10.1093/jxb/erp096
769 Lee, H., Park, J., Cho, S., Lee, M., Kim, H.S., 2019. Impact of leaf area index from various
770 sources on estimating gross primary production in temperate forests using the
771 JULES land surface model. Agric. For. Meteorol. 276–277, 107614.
772 https://doi.org/10.1016/j.agrformet.2019.107614
773 Lemordant, L., Gentine, P., Swann, A.S., Cook, B.I., Scheff, J., 2018. Critical impact of
774 vegetation physiology on the continental hydrologic cycle in response to increasing
775 CO2. Proc. Natl. Acad. Sci. 115, 4093–4098.
776 https://doi.org/10.1073/pnas.1720712115
777 Leuzinger, S., Körner, C., 2007. Water savings in mature deciduous forest trees under
778 elevated CO2. Glob. Change Biol. 13, 2498–2508. https://doi.org/10.1111/j.1365-
779 2486.2007.01467.x
780 Liu, J., You, Y., Li, J., Sitch, S., Gu, X., Nabel, J.E.M.S., Lombardozzi, D., Luo, M., Feng, X.,
781 Arneth, A., Jain, A.K., Friedlingstein, P., Tian, H., Poulter, B., Kong, D., 2021.
782 Response of global land evapotranspiration to climate change, elevated CO2, and
783 land use change. Agric. For. Meteorol. 311, 108663.
784 https://doi.org/10.1016/j.agrformet.2021.108663
785 Long, S.P., 1991. Modification of the response of photosynthetic productivity to rising
786 temperature by atmospheric CO2 concentrations: Has its importance been
787 underestimated? Plant Cell Environ. 14, 729–739. https://doi.org/10.1111/j.1365-
788 3040.1991.tb01439.x
789 Lundberg, S., Lee, S.-I., 2017. A Unified Approach to Interpreting Model Predictions.
790 ArXiv170507874 Cs Stat.
791 Lundberg, S.M., Erion, G., Chen, H., DeGrave, A., Prutkin, J.M., Nair, B., Katz, R.,
792 Himmelfarb, J., Bansal, N., Lee, S.-I., 2020. From local explanations to global
793 understanding with explainable AI for trees. Nat. Mach. Intell. 2, 56–67.
794 https://doi.org/10.1038/s42256-019-0138-9
795 Maurer, G.E., Hallmark, A.J., Brown, R.F., Sala, O.E., Collins, S.L., 2020. Sensitivity of

primary production to precipitation across the United States. Ecol. Lett. 23, 527–536. https://doi.org/10.1111/ele.13455

McCarthy, H.R., Oren, R., Finzi, A.C., Johnsen, K.H., 2006. Canopy leaf area constrains [CO2]-induced enhancement of productivity and partitioning among aboveground carbon pools. Proc. Natl. Acad. Sci. 103, 19356–19361. https://doi.org/10.1073/pnas.0609448103

McCarthy, H.R., Oren, R., Johnsen, K.H., Gallet-Budynek, A., Pritchard, S.G., Cook, C.W., LaDeau, S.L., Jackson, R.B., Finzi, A.C., 2010. Re-assessment of plant carbon dynamics at the Duke free-air CO2 enrichment site: interactions of atmospheric [CO2] with nitrogen and water availability over stand development. New Phytol. 185, 514–528. https://doi.org/10.1111/j.1469-8137.2009.03078.x

Medlyn, B.E., Barton, C.V.M., Broadmeadow, M.S.J., Ceulemans, R., De Angelis, P., Forstreuter, M., Freeman, M., Jackson, S.B., Kellomäki, S., Laitat, E., Rey, A., Roberntz, P., Sigurdsson, B.D., Strassemeyer, J., Wang, K., Curtis, P.S., Jarvis, P.G., 2001. Stomatal conductance of forest species after long-term exposure to elevated CO2 concentration: a synthesis. New Phytol. 149, 247–264. https://doi.org/10.1046/j.1469-8137.2001.00028.x

Medlyn, B.E., Duursma, R.A., Eamus, D., Ellsworth, D.S., Prentice, I.C., Barton, C.V.M., Crous, K.Y., Angelis, P.D., Freeman, M., Wingate, L., 2011. Reconciling the optimal and empirical approaches to modelling stomatal conductance. Glob. Change Biol. 17, 2134–2144. https://doi.org/10.1111/j.1365-2486.2010.02375.x

Meehl, G.A., Moss, R., Taylor, K.E., Eyring, V., Stouffer, R.J., Bony, S., Stevens, B., 2014. Climate Model Intercomparisons: Preparing for the Next Phase. Eos Trans. Am. Geophys. Union 95, 77–78. https://doi.org/10.1002/2014EO090001

Migliavacca, M., Musavi, T., Mahecha, M.D., Nelson, J.A., Knauer, J., Baldocchi, D.D., Perez-Priego, O., Christiansen, R., Peters, J., Anderson, K., Bahn, M., Black, T.A., Blanken, P.D., Bonal, D., Buchmann, N., Caldararu, S., Carrara, A., Carvalhais, N., Cescatti, A., Chen, J., Cleverly, J., Cremonese, E., Desai, A.R., El-Madany, T.S.,

824 Farella, M.M., Fernández-Martínez, M., Filippa, G., Forkel, M., Galvagno, M.,
825 Gomarasca, U., Gough, C.M., Göckede, M., Ibrom, A., Ikawa, H., Janssens, I.A.,
826 Jung, M., Kattge, J., Keenan, T.F., Knohl, A., Kobayashi, H., Kraemer, G., Law, B.E.,
827 Liddell, M.J., Ma, X., Mammarella, I., Martini, D., Macfarlane, C., Matteucci, G.,
828 Montagnani, L., Pabon-Moreno, D.E., Panigada, C., Papale, D., Pendall, E.,
829 Penuelas, J., Phillips, R.P., Reich, P.B., Rossini, M., Rotenberg, E., Scott, R.L.,
830 Stahl, C., Weber, U., Wohlfahrt, G., Wolf, S., Wright, I.J., Yakir, D., Zaehle, S.,
831 Reichstein, M., 2021. The three major axes of terrestrial ecosystem function. Nature
832 598, 468–472. https://doi.org/10.1038/s41586-021-03939-9
833 Miguez-Macho, G., Fan, Y., 2021. Spatiotemporal origin of soil water taken up by vegetation.
834 Nature 598, 624–628. https://doi.org/10.1038/s41586-021-03958-6
835 Norby, R.J., DeLucia, E.H., Gielen, B., Calfapietra, C., Giardina, C.P., King, J.S., Ledford, J.,
836 McCarthy, H.R., Moore, D.J.P., Ceulemans, R., Angelis, P.D., Finzi, A.C., Karnosky,
837 D.F., Kubiske, M.E., Lukac, M., Pregitzer, K.S., Scarascia-Mugnozza, G.E.,
838 Schlesinger, W.H., Oren, R., 2005. Forest response to elevated CO2 is conserved
839 across a broad range of productivity. Proc. Natl. Acad. Sci. 102, 18052–18056.
840 https://doi.org/10.1073/pnas.0509478102
841 Norby, R.J., Wullschleger, S.D., Gunderson, C.A., Johnson, D.W., Ceulemans, R., 1999.
842 Tree responses to rising CO2 in field experiments: implications for the future forest.
843 Plant Cell Environ. 22, 683–714. https://doi.org/10.1046/j.1365-3040.1999.00391.x
844 Norby, R.J., Zak, D.R., 2011. Ecological Lessons from Free-Air CO2 Enrichment (FACE)
845 Experiments. Annu. Rev. Ecol. Evol. Syst. 42, 181–203.
846 https://doi.org/10.1146/annurev-ecolsys-102209-144647
847 Novick, K.A., Ficklin, D.L., Stoy, P.C., Williams, C.A., Bohrer, G., Oishi, A.C., Papuga, S.A.,
848 Blanken, P.D., Noormets, A., Sulman, B.N., Scott, R.L., Wang, L., Phillips, R.P.,
849 2016. The increasing importance of atmospheric demand for ecosystem water and
850 carbon fluxes. Nat. Clim. Change 6, 1023–1027.
851 https://doi.org/10.1038/nclimate3114

852 Pedregosa, F., Varoquaux, G., Gramfort, A., Michel, V., Thirion, B., Grisel, O., Blondel, M.,
853 Prettenhofer, P., Weiss, R., Dubourg, V., Vanderplas, J., Passos, A., Cournapeau,
854 D., n.d. Scikit-learn: Machine Learning in Python. Mach. Learn. PYTHON 6.
855 Peñuelas, J., Canadell, J.G., Ogaya, R., 2011. Increased water-use efficiency during the
856 20th century did not translate into enhanced tree growth. Glob. Ecol. Biogeogr. 20,
857 597–608. https://doi.org/10.1111/j.1466-8238.2010.00608.x
858 Reichstein, M., Bahn, M., Ciais, P., Frank, D., Mahecha, M.D., Seneviratne, S.I.,
859 Zscheischler, J., Beer, C., Buchmann, N., Frank, D.C., Papale, D., Rammig, A.,
860 Smith, P., Thonicke, K., van der Velde, M., Vicca, S., Walz, A., Wattenbach, M.,
861 2013. Climate extremes and the carbon cycle. Nature 500, 287–295.
862 https://doi.org/10.1038/nature12350
863 Saxton, K.E., Rawls, W.J., 2006. Soil Water Characteristic Estimates by Texture and
864 Organic Matter for Hydrologic Solutions. Soil Sci. Soc. Am. J. 70, 1569–1578.
865 https://doi.org/10.2136/sssaj2005.0117
866 Schimel, D., Stephens, B.B., Fisher, J.B., 2015. Effect of increasing CO2 on the terrestrial
867 carbon cycle. Proc. Natl. Acad. Sci. 112, 436–441.
868 https://doi.org/10.1073/pnas.1407302112
869 Street, L.E., Shaver, G.R., Williams, M., Van Wijk, M.T., 2007. What is the relationship
870 between changes in canopy leaf area and changes in photosynthetic CO2 flux in
871 arctic ecosystems? J. Ecol. 95, 139–150. https://doi.org/10.1111/j.1365-
872 2745.2006.01187.x
873 Thum, T., Caldararu, S., Engel, J., Kern, M., Pallandt, M., Schnur, R., Yu, L., Zaehle, S.,
874 2019. A new model of the coupled carbon, nitrogen, and phosphorus cycles in the
875 terrestrial biosphere (QUINCY v1.0; revision 1996). Geosci. Model Dev. 12, 4781–
876 4802. https://doi.org/10.5194/gmd-12-4781-2019
877 Ueyama, M., Ichii, K., Kobayashi, H., Kumagai, T., Beringer, J., Merbold, L., Euskirchen,
878 E.S., Hirano, T., Marchesini, L.B., Baldocchi, D., Saitoh, T.M., Mizoguchi, Y., Ono, K.,
879 Kim, J., Varlagin, A., Kang, M., Shimizu, T., Kosugi, Y., Bret-Harte, M.S., Machimura,

T., Matsuura, Y., Ohta, T., Takagi, K., Takanashi, S., Yasuda, Y., 2020. Inferring CO2 fertilization effect based on global monitoring land-atmosphere exchange with a theoretical model. Environ. Res. Lett. 15, 084009. https://doi.org/10.1088/1748-9326/ab79e5

van der Sleen, P., Groenendijk, P., Vlam, M., Anten, N.P.R., Boom, A., Bongers, F., Pons, T.L., Terburg, G., Zuidema, P.A., 2015. No growth stimulation of tropical trees by 150 years of CO2 fertilization but water-use efficiency increased. Nat. Geosci. 8, 24–28. https://doi.org/10.1038/ngeo2313

Walker, A.P., De Kauwe, M.G., Medlyn, B.E., Zaehle, S., Iversen, C.M., Asao, S., Guenet, B., Harper, A., Hickler, T., Hungate, B.A., Jain, A.K., Luo, Y., Lu, X., Lu, M., Luus, K., Megonigal, J.P., Oren, R., Ryan, E., Shu, S., Talhelm, A., Wang, Y.-P., Warren, J.M., Werner, C., Xia, J., Yang, B., Zak, D.R., Norby, R.J., 2019. Decadal biomass increment in early secondary succession woody ecosystems is increased by CO2 enrichment. Nat. Commun. 10, 454. https://doi.org/10.1038/s41467-019-08348-1

Walker, A.P., Kauwe, M.G.D., Bastos, A., Belmecheri, S., Georgiou, K., Keeling, R.F., McMahon, S.M., Medlyn, B.E., Moore, D.J.P., Norby, R.J., Zaehle, S., Anderson-Teixeira, K.J., Battipaglia, G., Brienen, R.J.W., Cabugao, K.G., Cailleret, M., Campbell, E., Canadell, J.G., Ciais, P., Craig, M.E., Ellsworth, D.S., Farquhar, G.D., Fatichi, S., Fisher, J.B., Frank, D.C., Graven, H., Gu, L., Haverd, V., Heilman, K., Heimann, M., Hungate, B.A., Iversen, C.M., Joos, F., Jiang, M., Keenan, T.F., Knauer, J., Körner, C., Leshyk, V.O., Leuzinger, S., Liu, Y., MacBean, N., Malhi, Y., McVicar, T.R., Penuelas, J., Pongratz, J., Powell, A.S., Riutta, T., Sabot, M.E.B., Schleucher, J., Sitch, S., Smith, W.K., Sulman, B., Taylor, B., Terrer, C., Torn, M.S., Treseder, K.K., Trugman, A.T., Trumbore, S.E., Mantgem, P.J. van, Voelker, S.L., Whelan, M.E., Zuidema, P.A., 2021. Integrating the evidence for a terrestrial carbon sink caused by increasing atmospheric CO2. New Phytol. 229, 2413–2445. https://doi.org/10.1111/nph.16866

Way, D.A., Katul, G.G., Manzoni, S., Vico, G., 2014. Increasing water use efficiency along

the C3 to C4 evolutionary pathway: a stomatal optimization perspective. J. Exp. Bot. 65, 3683–3693. https://doi.org/10.1093/jxb/eru205

Weisstein, Eric W. (n.d."Least Squares Fitting." From MathWorld--A Wolfram Web Resource. https://mathworld.wolfram.com/LeastSquaresFitting.html

Williams, I.N., Torn, M.S., 2015. Vegetation controls on surface heat flux partitioning, and land-atmosphere coupling. Geophys. Res. Lett. 42, 9416–9424. https://doi.org/10.1002/2015GL066305

Winkler, A.J., Myneni, R.B., Hannart, A., Sitch, S., Haverd, V., Lombardozzi, D., Arora, V.K., Pongratz, J., Nabel, J.E.M.S., Goll, D.S., Kato, E., Tian, H., Arneth, A., Friedlingstein, P., Jain, A.K., Zaehle, S., Brovkin, V., 2021. Slowdown of the greening trend in natural vegetation with further rise in atmospheric CO_2. Biogeosciences 18, 4985–5010. https://doi.org/10.5194/bg-18-4985-2021

Woodward, F.I., Kelly, C.K., 1995. The influence of CO2 concentration on stomatal density. New Phytol. 131, 311–327. https://doi.org/10.1111/j.1469-8137.1995.tb03067.x

Wullschleger, S.D., Tschaplinski, T.J., Norby, R.J., 2002. Plant water relations at elevated CO2– implications for water-limited environments. Plant Cell Environ. 25, 319–331. https://doi.org/10.1046/j.1365-3040.2002.00796.x

Zaehle, S., Friend, A.D., 2010. Carbon and nitrogen cycle dynamics in the O-CN land surface model: 1. Model description, site-scale evaluation, and sensitivity to parameter estimates. Glob. Biogeochem. Cycles 24. https://doi.org/10.1029/2009GB003521